Self-Assembly and Photophysical Properties of Lanthanide Dinuclear Triple-Helical Complexes

Claude Piguet,*,† Jean-Claude G. Bünzli,*,‡ Gérald Bernardinelli,§ Gérard Hopfgartner,⊥ and Alan F. Williams†

Contribution from the Department of Inorganic, Analytical and Applied Chemistry, and the Laboratory of X-ray Crystallography, University of Geneva, CH-1211 Geneva 4, Switzerland, the Institute of Analytical and Inorganic Chemistry, University of Lausanne, CH-1005 Lausanne, Switzerland, and Pharma Division, Hoffmann-La Roche, CH-4002 Basel, Switzerland

Received May 10, 1993

Abstract: The dinucleating ligand bis[1-methyl-2-(6′-[1″-(3,5-dimethoxybenzyl)benzimidazol-2″-yl]pyrid-2′-yl)benzimidazol-5-yl]methane (L) reacts with lanthanide perchlorates to give dinuclear 2:3 complexes $[Ln_2(L)_3]^{6+}$ (Ln = La, Eu, Gd, Tb, and Lu). Detailed ES–MS, ^{1}H-NMR, luminescence, and spectrophotometric measurements in acetonitrile show that the cations $[Ln_2(L)_3]^{6+}$ are produced by strict self-assembly and adopt a triple-helical structure in solution (pseudo-D_3 symmetry). The crystal structure of $[Eu_2(L)_3](ClO_4)_6(CH_3CN)_9$ (**11**, $Eu_2C_{195}H_{177}N_{39}O_{36}Cl_6$, a = 17.634(3) Å, b = 21.408(4) Å, c = 29.437(7) Å, α = 82.13(1)°, β = 85.76(1)°, γ = 89.79(1)°, triclinic, $P\bar{1}$, Z = 2) shows a dinuclear pseudo-D_3 triple-helical cation, $[Eu_2(L)_3]^{6+}$, where the three bis(terdentate) ligands L are wrapped around the helical axis defined by the europium atoms. The Eu(III) of each site is 9-coordinated by six nitrogen atoms of the benzimidazole units occupying the vertices and three nitrogen atoms of the pyridine units occupying the capping positions of a slightly distorted, tricapped trigonal prism. Luminescence studies of the crystalline complex $[Eu_2(L)_3](ClO_4)_6 \cdot n$solv ($n$ = 9, solv = CH_3CN, **11**; n = 2, solv = H_2O, **6**; n = 9, solv = H_2O, **7**) confirm the pseudo-D_3 symmetry of the Eu(III) sites in **11** and show that secondary interactions with water molecules in **6** and **7** destroy the trigonal symmetry. An efficient intramolecular energy transfer between the $^3\pi\pi^*$ excited state centered on L and the excited levels of Eu(III) and Tb(III) is observed (antenna effect) together with a dipole–dipolar Tb → Eu intramolecular energy transfer in the heterodinuclear-doped Eu–Tb compound. Stability constants and ^{1}H NMR in acetonitrile show that the homodinuclear complexes $[Ln_2(L)_3]^{6+}$ are less stable for the heavier lanthanides Tb and Lu. The origin of this effect is discussed together with the nonstatistical distribution of the different species observed when stoichiometric quantities of L (3 equiv) are mixed with $Ln^1(ClO_4)_3$ (1 equiv) and $Ln^2(ClO_4)_3$ (1 equiv) in solution ($Ln^1 \neq Ln^2$; Ln^1 = La, Eu, Tb, and Lu; Ln^2 = Tb and Lu).

Introduction

The development of luminescent chemical probes and sensors is the subject of intensive research, both in natural[1] and medical[2] sciences. Probes based on Eu(III) and Tb(III) ions are of special interest because of the particularly suitable spectroscopic properties of these ions.[3] Moreover, it has been realized that trivalent lanthanide ions may be incorporated in supramolecular complexes acting as molecular photonic devices.[4] In some of these devices, which work on the nanometric scale, the various steps of the overall process involving absorption of light, transfer, and reemission at another wavelength are performed separately by distinct parts of the complex. Such supramolecular constructions are termed *light-conversion molecular devices*. To design a good lanthanide luminescent sensor, a unique combination of features must be realized: (i) protection of the included ion from quenching due to the interaction with solvent molecules and/or high-energy vibrations from the ligating groups, (ii) presence of multiple absorbing groups suitable for energy transfer (antenna effect[4]), and (iii) high thermodynamic stability and kinetic inertness. Typical examples are lanthanide cryptates based on bipyridyl units[4,5] or containing *N*-oxide groups.[4,6]

The yield of the energy transfer between the donor (the emitter) and the acceptor is related to the donor–acceptor distance. The determination of this distance allows one to realize a fluorescent mapping of large molecules such as proteins, leading to useful structural information, or to calculate the distance between metal ion sites.[3] In order to unravel the intimate mechanism of energy-transfer processes both between an organic chromophore and a Ln(III) ion and between two lanthanide ions, we have undertaken a study of several classes of heterodinuclear complexes.[7,8] A major difficulty is the frequent formation of a statistical combination of homo- and heterodinuclear complexes, requiring a more complicated interpretation of the photophysical measurements. The use of building blocks for the self-assembly of large complexes with specific properties is a promising technique. It has recently been used sucessfully to design helical dinuclear complexes in which two lanthanide ions can be included at a distance of 8.9 Å.[9] Since the nature of these ligand groups can be easily modified,[10] we hope to be able to alter them in order to get true heterodinuclear species and, in addition, efficient energy conversion and transfer.

† Department of Inorganic, Analytical and Applied Chemistry, Geneva.
‡ Institute of Analytical and Inorganic Chemistry, Lausanne.
§ Laboratory of X-ray Crystallography, Geneva.
⊥ Hoffmann-La Roche, Pharma Division, Basel.

(1) Tangay, J. F.; Suib, S. L. *Catal. Rev. Sci. Eng.* **1987**, *29*, 1.
(2) Leiner, M. J. P. *Anal. Chim. Acta* **1991**, *255*, 209.
(3) Choppin, G. R.; Bünzli, J.-C. G. *Lanthanide Probes in Life, Chemical and Earth Sciences*; Elsevier Publishing Co.: Amsterdam, 1989; Chapter 7.
(4) Lehn, J.-M. In *Frontiers in Supramolecular Organic Chemistry and Photochemistry*; Schneider, H.-J., Dürr, H., Eds.; VCH: Weinheim, 1991; pp 1–28. Sabbatini, N.; Guardigli, M.; Lehn, J.-M. *Coord. Chem. Rev.* **1993**, *123*, 201.
(5) Blasse, G.; Dirksen, G. J.; Van der Voort, D.; Sabbatini, N.; Perathoner, S. *Chem. Phys. Lett.* **1988**, 387.
(6) Roth, C. O. Ph.D. Thesis, Université Louis Pasteur, Strasbourg, 1992.
(7) Guerriero, P.; Vigato, P. A.; Bünzli, J.-C. G.; Moret, E. *J. Chem. Soc., Dalton Trans.* **1990**, 647.
(8) Froidevaux, P. Ph.D. Thesis, Université de Lausanne, 1992.
(9) Bernardinelli, G.; Piguet, C.; Williams, A. F. *Angew. Chem., Int. Ed. Engl.* **1992**, *12*, 1622.
(10) Bochet, C. G.; Piguet, C.; Williams, A. F. *Helv. Chim. Acta* **1993**, *76*, 372.

0002-7863/93/1515-8197$04.00/0

Chart I

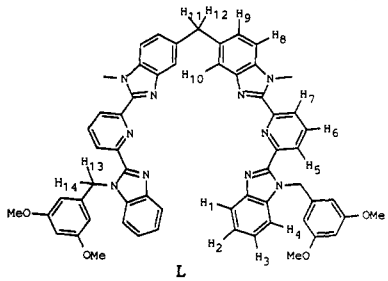

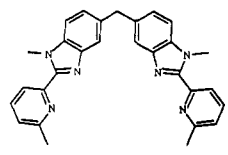

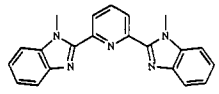

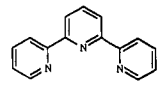

In this paper, we present the synthesis of the new dinucleating bis(terdentate) ligand bis[1-methyl-2-[6′-(1″-(3,5-dimethoxybenzyl)benzimidazol-2″-yl)pyrid-2′-yl]benzimidazol-5-yl]methane (L) which corresponds to two mbzimpy terdentate units linked by a methylene bridge (Chart I) and the self-assembly and structural and photophysical properties of 2:3 complexes with triple-helical structure obtained from L and lanthanide perchlorates: $[Ln_2L_3](ClO_4)_6 \cdot n$solv (Ln = La, Eu, Gd, Tb, and Lu; solv = CH_3CN and H_2O; **5–11**).

Experimental Section

Solvents and starting materials were purchased from Fluka AG (Buchs, Switzerland) and used without further purification, unless otherwise stated. Aluminum oxide (Merck activity II-III, 0.063–0.200 mm) was used for preparative column chromatography.

Spectroscopic and Analytical Measurements. Reflectance spectra were recorded on a Perkin-Elmer-Hitachi 340 spectrometer as finely ground powders dispersed in MgO (5%), with MgO as reference. Electronic spectra in the UV–visible range were recorded at 22 °C in acetonitrile solution with a Perkin-Elmer Lambda 7 spectrometer using quartz cells of 1- and 0.1-cm path length. Spectrophotometric titrations were performed with a Perkin-Elmer Lambda 5 spectrophotometer connected to an external computer. In a typical experiment, 50 mL of ligand (L) in acetonitrile (10^{-4} M) was titrated with a 2.5×10^{-3} M solution of the perchlorate salt of the appropriate metal ion [La(III), Eu(III), Lu(III)] in acetonitrile. After each addition of 0.20 mL, the absorbances at 10 different wavelengths were recorded using a 0.1-cm quartz cell and transferred to the computer. Plots of extinction as a function of the metal/ligand ratio gave a first indication of the number and stoichiometry of the complexes formed; factor analysis[20] was then applied to the data to confirm the number of different absorbing species. Finally, a model for the distribution of species was fitted with a nonlinear least-squares algorithm to give stability constants as previously described.[11] IR spectra were obtained from KBr pellets with a Bruker IFS 113v FT IR spectrometer. Raman spectra were recorded on a Ramalog-4 spectrometer from Spex Industries under excitation by an Ar laser. ^{1}H-NMR and ^{13}C-NMR spectra were recorded on Varian XL 200 and Bruker AMX 400 spectrometers. Chemical shifts are given in parts per million with reference to TMS. Abbreviations are as follows: s, singlet; d, doublet; dd, doublet of doublets; t, triplet; and m, multiplet. EI–MS (70 eV) were recorded with VG 7000E and Finnigan 4000 instruments. FAB–MS (positive mode from nitrobenzyl alcohol matrix) were recorded at the Laboratory of Mass Spectrometry of the University of Strasbourg (France). ES–MS mass spectra were recorded on an API-III tandem triple quadrupole mass spectrometer system (Sciex, Toronto, Ontario, Canada) by infusion at 4–10 μL/min. The spectra were recorded under low upfront declustering or collision induced dissociation (CID) conditions,[21] typically $\Delta V = 10$–50 V between the orifice and the first quadrupole of the Sciex. Luminescence measurements were performed on a previously described instrumental setup.[7,8,22] To remove water, acetonitrile solutions were treated with 3-Å molecular sieves prior to measurement. Solid-state samples were finely powdered, except for some of the Eu and Tb crystals with no hydration water, which were measured in Et_2O. Luminescence spectra are corrected for the instrumental function, but excitation spectra are not. Lifetimes are averages of at least three independent determinations. Elemental analyses were performed by Dr. H. Eder of the Microchemical Laboratory of the University of Geneva.

Preparation of the Ligands. 3,3′-Diamino-4,4′-bis(*N*-methylamino)-diphenylmethane (**1**)[11] and 2-(2-benzimidazolyl)-6-methylpyridine (**2**)[12] were prepared according to literature procedures.

Preparation of 2-(2-Benzimidazolyl)-6-carboxypyridine (3). 2-(2-Benzimidazolyl)-6-methylpyridine (**2**, 30.8 g, 0.147 mol) and selenium dioxide (73.6 g, 0.663 mol) were refluxed in dry pyridine for 36 h. After cooling, the mixture was filtered to remove solid Se and the clear solution was evaporated to dryness. The crude residue was suspended in water (150 mL), and the pH was adjusted to 11.0 with NaOH (5 M). The resulting clear, yellow solution was extracted with dichloromethane (3 × 75 mL), and the aqueous phase was filtered and neutralized to pH = 3.4 with concentrated hydrochloric acid. The precipitate was collected by filtration and crystallized from dimethyl sulfoxide/water 1:1 (100 °C) to give 31 g (0.121 mol, yield = 82%) of 2-(2-benzimidazolyl)-6-carboxypyridine monohydrate (**3**), mp > 200 °C. ^{1}H NMR in DMSO-d_6: δ 7.3–7.7 (4H, m, AA′BB′), 8.18 (1H, dd, $J^3 = 7$ Hz, $J^4 = 1.5$ Hz), 8.22 (1H, t, $J^3 = 7$ Hz), 8.55 (1H, dd, $J^3 = 7$ Hz, $J^4 = 1.5$ Hz), 13.0 (1H, s). EI–MS: 239 (M^+), 195 ($[M - CO_2]^+$). Anal. Calcd for $C_{13}H_9N_3O_2 \cdot H_2O$: C, 60.70; N, 16.34; H, 4.28. Found: C, 61.46; N, 16.49; H, 4.16.

Preparation of Bis[1-methyl-2-(6′-[benzimidazol-2″-yl]pyrid-2′-yl)-benzimidazol-5-yl]methane (4). 3,3′-Diamino-4,4′-bis(*N*-methylamino)-diphenylmethane (**1**, 3.33 g, 13 mmol) and 2-(2-benzimidazolyl)-6-carboxypyridine (**3**, 7.02 g, 27.3 mmol) were dissolved in concentrated phosphoric acid (85%, 200 mL), slowly heated to 180 °C, and maintained at this temperature for 2 h. After cooling, the mixture was poured into water (500 mL) and neutralized to pH = 2.0 with NaOH (5 M). The precipitate was filtered, washed with water (300 mL), and suspended in warm (60 °C) aqueous potassium carbonate (10%, 500 mL) for 1 h. The purple precipitate was separated by filtration, washed with water, and crystallized from dimethyl sulfoxide/water (charcoal) to give 5.5 g (8.3 mmol, yield = 64%) of bis[1-methyl-2-(6′-[benzimidazol-2″-yl]pyrid-2′-yl)benzimidazol-5-yl]methane (**4**), mp > 200 °C. ^{1}H NMR in DMSO-d_6: δ 4.24 (2H, s), 4.31 (6H, s), 7.2–7.4 (6H, m), 7.6–7.8 (8H, m), 8.16 (2H, t, $J^3 = 8$ Hz), 8.29 (2H, dd, $J^3 = 8$ Hz, $J^4 = 1.5$ Hz), 8.42 (2H, dd, $J^3 = 8$ Hz, $J^4 = 1.5$ Hz), 12.8 (2H, s). FAB–MS: 663 ($[M + H]^+$).

Preparation of Bis[1-methyl-2-(6′-[1″-(3,5-dimethoxybenzyl)benzimidazol-2″-yl]pyrid-2′-yl)benzimidazol-5-yl]methane (L). Bis[1-methyl-2-(6′-[benzimidazol-2″-yl]pyrid-2′-yl)benzimidazol-5-yl]methane (**4**, 1 g, 1.51 mmol) was dissolved in dry DMF (130 mL, distilled from CaH_2) under an inert atmosphere and cooled to 0 °C. NaH (181 mg, 60% dispersion in oil, 4.53 mmol) was added, and the mixture was allowed to stir at room temperature for 1 h. 3,5-Dimethoxybenzyl bromide[13] (1.05 g, 4.53 mmol) in DMF (15 mL) was added, and the resulting mixture was stirred for 15 h and poured into water (400 mL). The precipitate was filtered, dissolved in dichloromethane (200 mL), and dried over sodium sulfate, and the organic phase was evaporated to dryness. The crude residue was purified by column chromatography (Al_2O_3, CH_2Cl_2/MeOH 99.5:0.5) to give 1.35 g (1.35 mmol, yield = 89%) of bis[1-methyl-2-(6′-[1″-(3,5-dimethoxybenzyl)benzimidazol-2″-yl]pyrid-2′-yl)benzimidazol-5-yl]methane dihydrate (**L**) as a pale yellow powder, mp = 168–170 °C. ^{1}H NMR in $CDCl_3$: δ 3.59 (12H, s), 3.68 (6H, s), 4.28 (2H, s), 5.82 (4H, s), 6.18 (4H, d, $J^4 = 2$ Hz), 6.30 (2H, t, $J^4 = 2$ Hz), 7.2–7.4 (10H, m), 7.69 (2H, s), 7.88 (2H, m), 8.02 (2H, t, $J^3 = 8$ Hz), 8.30 (2H, dd, $J^3 = 8$ Hz, $J^4 = 1.5$ Hz), 8.44 (2H, dd, $J^3 = 8$ Hz, $J^4 = 1.5$ Hz). ^{13}C NMR in $CDCl_3$: δ 31.59, 55.10 (primary C); 42.20, 48.76 (secondary C); 99.14, 104.24, 109.84, 110.84, 119.88, 120.25, 123.05, 123.87, 124.88, 125.38, 125.51, 138.02 (tertiary C); 135.55, 136.57, 136.70, 139.51, 142.68, 142.83, 149.50, 149.68, 150.05, 150.30, 161.10 (quaternary C). EI–MS: 963 (M^+). Anal. Calcd for $C_{59}H_{50}N_{10}O_4 \cdot 2H_2O$: C, 70.93; N, 14.02; H, 5.45. Found: 71.15; N, 13.89; H, 5.19.

(11) Piguet, C.; Bernardinelli, G.; Bocquet, B.; Quattropani, A.; Williams, A. F. *J. Am. Chem. Soc.* **1992**, *114*, 7440.
(12) Barni, E.; Savarino, P. *J. Heterocycl. Chem.* **1977**, *14*, 937.
(13) Rüttimann, S.; Piguet, C.; Bernardinelli, G.; Bocquet, B.; Williams, A. F. *J. Am. Chem. Soc.* **1992**, *114*, 4230.

Preparation of Lanthanide Complexes. The perchlorate salts $Ln(ClO_4)_3 \cdot nH_2O$ (n = 6–8) were prepared from the corresponding oxide (Glucydur, 99.99%) according to a literature method.[14]

Preparation of $[Ln_2(L)_3](ClO_4)_6 \cdot xH_2O \cdot yCH_3CN$ (Ln = La, 5; Eu, 6–7; Gd, 8; Tb, 9; and Lu, 10). $Ln(ClO_4)_3 \cdot nH_2O$ (n = 6–8) (0.035 mmol) in acetonitrile (10 mL) was slowly added to a solution of L (50 mg, 0.052 mmol) in acetonitrile/dichloromethane 1:1 (10 mL). The resulting yellow solution was evaporated to dryness and dissolved in acetonitrile, and diethyl ether was allowed to diffuse into the solution for 3 days. The resulting yellow X-ray quality prisms were separated by filtration to give a 70–90% yield of $[Ln_2(L)_3](ClO_4)_6 \cdot xH_2O \cdot yCH_3CN$ [Ln = La, **5** (x = 2, y = 1); Eu, **6** (x = 2, y = 0); Eu, **7** (x = 9, y = 0); Gd, **8** (x = 2, y = 1); Tb, **9** (x = 3, y = 1); and Lu, **10** (x = 5, y = 0.5)]. The complex $[(Eu)(Tb)(L)_3](ClO_4)_6$ was prepared according to the same procedure using stoichiometric mixtures of lanthanide perchlorate salts. Complexes **5–10** were characterized by their IR spectra and gave satisfactory elemental analyses.

Caution! Perchlorate salts with organic ligands are potentially explosive and should be handled with the necessary precautions.[15]

Crystal Structure Determination of $[Eu_2(L)_3](ClO_4)_6 \cdot (CH_3CN)_9$ (11). $Eu_2C_{195}H_{177}N_{39}O_{36}Cl_6$: M_r = 4159.4, μ = 0.711 mm^{-1}, F_{000} = 4272, d_x = 1.26 g cm^{-3}; triclinic, $P\bar{1}$, Z = 2, a = 17.634(3) Å, b = 21.408(4) Å, c = 29.437(7) Å, α = 82.13(1)°, β = 85.76(1)°, γ = 89.79(1)°, V = 10978(4) Å^3 from 28 reflections (10° < 2θ < 20°). Crystal form: yellow prism 0.26 × 0.26 × 0.26 mm mounted in a capillary with mother liquor. Cell dimensions and intensities were measured at room temperature on a Philips PW1100 diffractometer with graphite-monochromated Mo Kα radiation, ω-2θ scans, scan width 1.2 + 0.2 tan(θ), and scan speed 0.06°/s; two reference reflections measured every 45 min showed a total decrease in intensity of 21% during the data collection. All intensities were corrected for this drift. $-16 < h < 16$; $-19 < k < 19$; $0 < l < 26$; 6° < 2θ < 38°. There were 17 573 measured reflections of which 8322 were observable ($|F_o| > 4\sigma(F_o)$). Data were corrected for Lorentz and polarization but not for absorption effects. The structure was solved by direct methods using MULTAN 87;[16] all other calculations used XTAL[17] system and ORTEP II[18] programs. Atomic scattering factors and anomalous dispersion terms were taken from ref 19. The six uncoordinated perchlorate anions and the six phenyl rings of the 3,5-dimethoxybenzyl substituents were refined as rigid groups, and, of the nine acetonitrile molecules, three were observed with three atomic sites, five with two atomic sites, and one with only one atomic site attributed to a nitrogen atom. Blocked matrix refinement was performed with four blocks (ligand A and europium, ligand B, ligand C, and perchlorate and solvent molecules; maximum number of variables = 1117). The europium and nitrogen atoms were refined with anisotropic thermal displacement parameters (32 atoms) and all the other atoms (239) with isotropic thermal displacement parameters. Eleven oxygen atoms of three perchlorate anions and four carbon atoms of 3,5-dimethoxybenzyl groups displayed too large atomic displacement parameters and were refined with site-occupancy factors smaller than 1 (Table SI, supplementary material). The final R factor is $R = R_w$ = 0.127 (w = 1) for 1117 variables and 8322 contributing reflections. The mean shift/error on the last cycle was 0.04 and the maximum 0.517. Coordinates of hydrogen atoms other than those of methoxy groups were calculated and contributed to F_c calculations. The final Fourier difference synthesis showed a maximum of 1.86 e Å^{-3} and a minimum of −4.91 e Å^{-3}. Negative residues of −4.91 and −3.89 e Å^{-3} are localized on Eu(1) and Eu(2), respectively. The relative large, final R value is still satisfactory if we consider the partial decomposition of the crystal during data collection and the observed disorder of the 3,5-dimethoxybenzyl groups, the perchlorate anions, and the acetonitrile molecules.

Scheme I

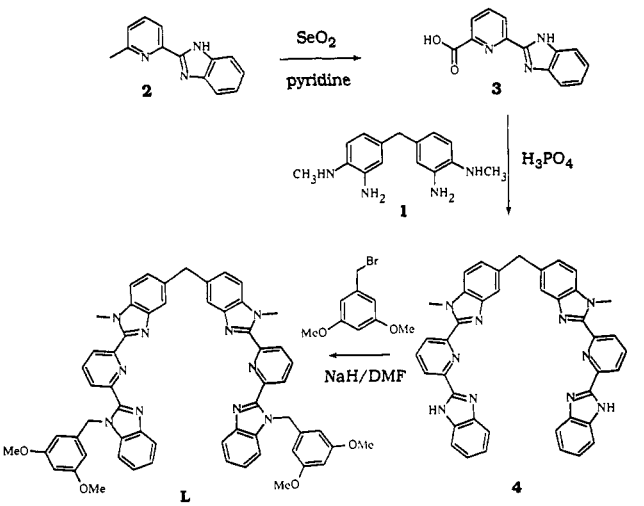

Results

The bis(terdentate) ligand bis[1-methyl-2-(6′-[1″-(3,5-dimethoxybenzyl)benzimidazol-2″-yl]pyrid-2′-yl)benzimidazol-5-yl]-methane (L) is obtained in three steps according to a strategy previously used for the preparation of the analogous bis(bidentate) ligand bismbmp[11] (Chart I). The poorly soluble precursor bis-[1-methyl-2-(6′-[benzimidazol-2″-yl]pyrid-2′-yl)benzimidazol-5-yl]methane (**4**) is synthesized using a modified double Philips reaction[23–25] between the tetraamine **1**[11] and 2-(2-benzimidazolyl)-6-carboxypyridine (**3**) (Scheme I). Alkylation with 3,5-dimethoxybenzyl bromide[13] gives a good yield of the lipophilic ligand L after careful chromatography of the dark, crude reaction product.

Preparation of Lanthanide Complexes 5–10. The Ln(III) complexes are prepared by mixing the ligand L with stoichiometric amounts of $Ln(ClO_4)_3 \cdot nH_2O$ (n = 6–8)[14] in dichloromethane/acetonitrile. The crude product may be recrystallized in good yield by slow diffusion of diethyl ether into a concentrated acetonitrile solution to give X-ray quality prisms. Nine acetonitrile molecules are found in the crystal structure of $[Eu_2(L)_3](ClO_4)_6(CH_3CN)_9$ (**11**, vide infra), but the prisms are slowly transformed into microcrystalline powders when separated from the mother liquor, and elemental analyses of the isolated products are compatible with the formulations $[Ln_2(L)_3](ClO_4)_6 \cdot xH_2O \cdot yCH_3CN$ [Ln = La, **5** (x = 2, y = 1); Eu, **6** (x = 2, y = 0; Eu, **7** (x = 9, y = 0); Gd, **8** (x = 2, y = 1); Tb, **9** (x = 3, y = 1); and Lu, **10** (x = 5, y = 0.5)]. The number of solvent molecules depends strongly on the drying conditions used during the synthesis and must be determined for each batch of crystals. The FAB–MS spectrum of complex **6** exhibits two peaks centered at m/z = 3690.0 and 3590.9 whose isotopic pattern corresponds to the species $[Eu_2(L)_3(ClO_4)_5]^+$ and $[Eu_2(L)_3(ClO_4)_4]^+$, respectively. The IR spectra show the characteristic ligand vibrations in the range of 1600–600 cm^{-1} for the complexes **5–10** together with peaks characteristic of the uncoordinated solvent molecules (3400 and 1620 cm^{-1} for H_2O and 2260 cm^{-1} for CH_3CN).[26] The ClO_4^- anions show the two vibrations (1095 and 625 cm^{-1}) typical of ionic perchlorate.[26]

(14) Desreux, J. F. In *Lanthanide Probes in Life, Chemical and Earth Sciences*; Choppin, G. R., Bünzli, J.-C. G., Eds.; Elsevier Publishing Co.: Amsterdam, 1989; Chapter 2, p 43.
(15) Wolsey, W. C. *J. Chem. Educ.* **1973**, *55*, A355.
(16) Main, P.; Fiske, S. J.; Hull, S. E.; Lessinger, L.; Germain, D.; Declercq, J. P.; Woolfson, M. M. MULTAN 87; Universities of York and Louvain-La-Neuve: York, England, and Louvain-La-Neuve, Belgium, 1987.
(17) Hall, S. R., Stewart, J. M., Eds. *XTAL 3.0 User's Manual*; Universities of Western Australia and Maryland, 1989.
(18) Johnson, C. K. ORTEP II, Report ORNL-5138; Oak Ridge National Laboratory: Oak Ridge, TN, 1976.
(19) *International Tables for X-ray Crystallography*; Kynoch Press: Birmingham, England, 1974; Vol. IV.
(20) Malinowski, E. R.; Howery, D. G. *Factor Analysis in Chemistry*; J. Wiley: New York, Chichester, Brisbane, and Toronto, 1980.
(21) Hopfgartner, G.; Bean, K.; Wachs, T.; Henion, J. D. *Anal. Chem.* **1993**, *56*, 439.
(22) Piguet, C.; Williams, A. F.; Bernardinelli, G.; Moret, E.; Bünzli, J.-C. G. *Helv. Chim. Acta* **1992**, *75*, 1697.
(23) Addison, A. W.; Burke, P. J. *J. Heterocycl. Chem.* **1981**, *18*, 803.
(24) Addison, A. W.; Rao, T. N.; Wahlgren, C. G. *J. Heterocycl. Chem.* **1983**, *20*, 1481.
(25) Piguet, C.; Bocquet, B.; Müller, E.; Williams, A. F. *Helv. Chim. Acta* **1989**, *72*, 323.
(26) Nakamoto, K. *Infrared and Raman Spectra of Inorganic and Coordination Compounds*, 3rd ed.; John Wiley: New-York-Chichester-Brisbane-Toronto, 1972, pp 142–154.

Table I. Selected Bond Distances (Å), and Bond Angles (Degrees), and Least-Squares Plane Data for $[Eu_2(L)_3](ClO_4)_6(CH_3CN)_9$ (11)

		distances				distances		
	distances	ligand A	ligand B	ligand C		ligand A	ligand B	ligand C
Eu(1)–Eu(2)	8.876(3)				Eu(2)–N(6)	2.57(3)	2.61(3)	2.61(3)
Eu(1)–N(1)		2.57(3)	2.58(3)	2.57(3)	Eu(2)–N(8)	2.58(3)	2.64(3)	2.58(3)
Eu(1)–N(3)		2.59(3)	2.59(3)	2.61(2)	Eu(2)–N(9)	2.67(3)	2.60(3)	2.59(3)
Eu(1)–N(4)		2.60(3)	2.58(2)	2.54(3)				

	angles[a]		angles[a]		angles[a]		angles[a]
	N(tbzim)–Eu–N(py) "bite angles"				N(py)–Eu–N(py)		
N(1a)–Eu(1)–N(3a)	61.6(9)	N(9a)–Eu(2)–N(8a)	62(1)	N(3a)–Eu(1)–N(3b)	124.2(8)	N(8a)–Eu(2)–N(8b)	124(1)
N(1b)–Eu(1)–N(3b)	61.9(8)	N(9b)–Eu(2)–N(8b)	62(1)	N(3b)–Eu(1)–N(3c)	117.5(8)	N(8b)–Eu(2)–N(8c)	116(1)
N(1c)–Eu(1)–N(3c)	61.5(9)	N(9c)–Eu(2)–N(8c)	62.4(9)	N(3a)–Eu(1)–N(3c)	118.2(9)	N(8a)–Eu(2)–N(8c)	120(1)
	N(py)–Eu–N(bzim) "bite angles"				N(bzim)–Eu–N(bzim)		
N(3a)–Eu(1)–N(4a)	64.2(9)	N(8a)–Eu(2)–N(6a)	62.8(9)	N(4a)–Eu(1)–N(4b)	85.9(9)	N(6a)–Eu(2)–N(6b)	85.8(9)
N(3b)–Eu(1)–N(4b)	62.7(8)	N(8b)–Eu(2)–N(6b)	64(1)	N(4b)–Eu(1)–N(4c)	83.5(8)	N(6b)–Eu(2)–N(6c)	84.9(9)
N(3c)–Eu(1)–N(4c)	65.1(8)	N(8c)–Eu(2)–N(6c)	62.4(8)	N(4a)–Eu(1)–N(4c)	85.3(9)	N(6a)–Eu(2)–N(6c)	84.4(8)
	N(tbzim)–Eu–N(tbzim)						
N(1a)–Eu(1)–N(1b)	86.3(9)	N(9a)–Eu(2)–N(9b)	86(1)				
N(1b)–Eu(1)–N(1c)	85.8(8)	N(9b)–Eu(2)–N(9c)	83(1)				
N(1a)–Eu(1)–N(1c)	83.7 (9)	N(9a)–Eu(2)–N(9c)	87.8(9)				

		deviations, Å				deviations, Å	
	least-squares planes description[b]	max	atom		least-squares planes description[b]	max	atom
tbA1	tbzim, N(1a), N(2a)	0.1	C(2a)	bB2	bzim, N(6b), N(7b)	0.08	C(22b)
pA1	py, N(3a)	0.03	C(9a)	pB2	py, N(8b)	0.03	C(32b)
bA1	bzim, N(4a), N(5a)	0.08	C(18a)	tbB2	tbzim, N(9b), N(10b)	0.12	C(36b)
bA2	bzim, N(6a), N(7a)	0.04	N(7a)	tbC1	tbzim, N(1c), N(2c)	0.06	C(4c)
pA2	py, N(8a)	0.03	C(29a)	pC1	py, N(3c)	0.02	C(8c)
tbA2	tbzim, N(9a), N(10a)	0.12	C(33a)	bC1	bzim, N(4c), N(5c)	0.05	C(19c)
tbB1	tbzim, N(1b), N(2b)	0.11	C(4b)	bC2	bzim, N(6c), N(7c)	0.1	C(21c)
pB1	py, N(3b)	0.03	C(10b)	pC2	py, N(8c)	0.05	C(30c)
bB1	bzim, N(4b), N(5b)	0.05	C(17b)	tbC2	tbzim, N(9c), N(10c)	0.06	C(38c)

	interplane angles																
	pA1	bA1	bA2	pA2	tbA2	tbB1	pB1	bB1	bB2	pB2	tbB2	tbC1	pC1	bC1	bC2	pC2	tbC2
tbA1	31	50	56	35	22	62	62	62	4	25	46	51	31	23	61	59	61
pA1		21	66	59	52	37	48	63	35	7	18	61	55	53	37	45	61
bA1			63	69	67	17	33	56	54	26	4	60	64	67	18	31	54
bA2				30	45	58	39	15	57	61	60	5	30	45	55	37	15
pA2					17	72	59	43	34	53	64	27	4	16	69	56	42
tbA2						75	67	57	20	45	63	41	15	1	73	64	55
tbB1							21	46	66	40	19	55	68	75	3	21	45
pB1								26	66	48	33	37	57	67	18	4	25
bB1									65	60	54	16	42	56	44	26	2
bB2										28	50	53	31	21	65	62	63
pB2											22	56	48	45	40	45	58
tbB2												57	60	63	19	31	52
tbC1													27	41	53	36	16
pC1														14	66	54	41
bC1															73	64	55
bC2																18	42
pC2																	24

[a] py = pyridine, bzim = benzimidazole, and tbzim = terminal benzimidazole. [b] The rings are denoted as pyridine p, benzimidazole b, or terminal benzimidazole tb, belonging to ligand strand A, B, or C and bound to Eu(1) or Eu(2). Thus, tbC1 is the terminal benzimidazole ring of strand C that is bound to Eu(1). The error in the dihedral angles between aromatic planes is typically 1°.

X-ray Crystal Structure of $[Eu_2(L)_3](ClO_4)_6(CH_3CN)_9$ (11). A partial report of the crystal structure of this complex has already been published.[9] Selected bond lengths, angles, and least-squares plane data are given in Table I. Figure 1 shows the atomic numbering scheme, and Figure 2 gives an ORTEP[18] stereoscopic view of the complex perpendicular to the helical axis.

In agreement with FAB–MS and IR data, the crystal structure of **11** shows the cation $[Eu_2(L)_3]^{6+}$, six uncoordinated perchlorate anions, and nine solvent molecules. The anions and the solvent molecules are disordered but otherwise show no feature of interest. In the dinuclear cation $[Eu_2(L)_3]^{6+}$, the ligands act as bis-(terdentate) units bound to the europium atoms and wrapped around the helical axis. This leads to a triple-helical structure with a pseudo-C_3 axis defined by the Eu(III) atoms which are separated by 8.876(3) Å. The coordination sites of the two europium atoms are very similar and may be described as slightly distorted, tricapped trigonal prisms with six benzimidazole nitrogen atoms occupying the vertices of the prism and the three pyridine nitrogen atoms occupying the capping positions, forming an intermediate plane containing the Eu(III) (deviation of Eu(III) from the plane: Eu(1), 0.010(2) Å; Eu(2), 0.019(6) Å). These planes are almost parallel (10.7(8)°), leading only to a weak bending of the structure. The Eu–N distances are very similar, within experimental error, with an average value of 2.59(6) Å. They correspond to those measured for the mononuclear 9-coordinated Eu(III) complexes $[Eu(terpy)_3](ClO_4)_3$ (2.60 Å)[27] and $[Eu(mbzimpy)_3](ClO_4)_3$ (2.59 Å).[28] Using Shannon's definition[29] and $r(N) = 1.46$ Å,[28] we calculate effective ionic

(27) Frost, G. H.; Hart, F. A.; Hursthouse, M. B. *J. Chem. Soc., Chem. Comm.* **1969**, 1421.
(28) Piguet, C.; Williams, A. F.; Bernardinelli, G.; Bünzli, J.-C. G. *Inorg. Chem.*, in press.

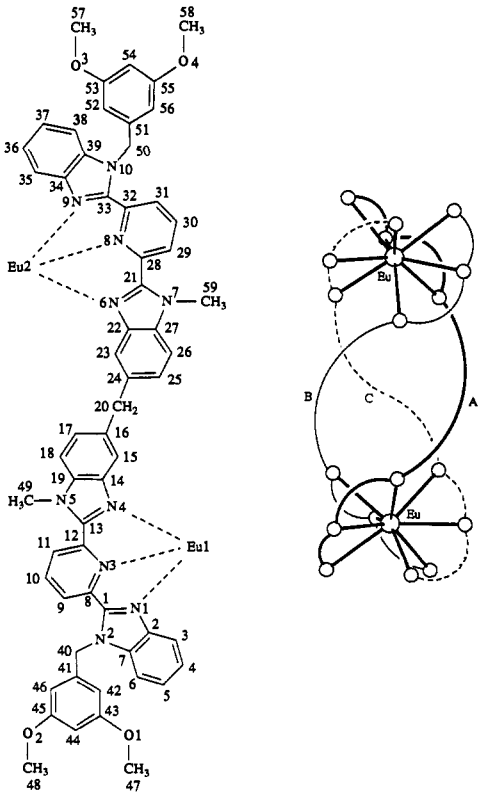

Figure 1. Atomic numbering scheme for $[Eu_2(L)_3]^{6+}$ (**11**).

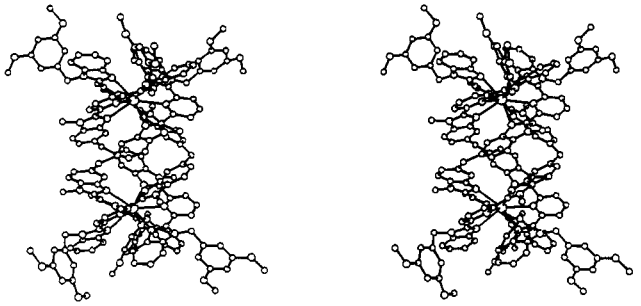

Figure 2. ORTEP[18] streoscopic view of the complex $[Eu_2(L)_3]^{6+}$ perpendicular to the helical axis.

radii for Eu(III) of 1.12 Å (Eu(1)) and 1.15 Å (Eu(2)), in agreement with the reported value for 9-coordinate Eu(III) complexes (1.12 Å)[3] which confirms the good fit between the ligand coordination cavities and Eu(III). As a result of the similar coordination and orientation of the ligands to Eu(III), we observe three pseudo-C_2 axes perpendicular to the pseudo-C_3 and passing through the methylene bridges, eventually leading to a pseudo-D_3 symmetry for the cation $[Eu_2(L)_3]^{6+}$. As previously described for helical complexes with polypyridines,[30] the helical twist within the ligands is achieved through rotations about the interannular C–C bonds. Within each terdentate unit bound to the europium atoms in $[Eu_2(L)_3]^{6+}$, the dihedral angles between the benzimidazole and pyridine rings are in the range of 14.4–31.3° (average value 23°) and close to the values reported for $[Eu(mbzimpy)_3]^{3+}$ (25.1–25.4°).[28] The main distortion responsible for the helical twist is found between the benzimidazole rings connected by the CH_2 bridges (63.2–73.3°, average 67.1°), as reported for the analogous triple-helical complex $[Co_2(bismbmp)_3]^{4+}$ (average dihedral angle 80°).[31] We observe weak stacking interactions between the nearly parallel central benzimidazole aromatic planes (Table I, bA1–bC2, bA2–bB1, bB2–bC1) belonging to different strands (angles 14.8–21°; distance between stacked planes 3.7–4.6 Å), but we find no strong stacking interactions between benzimidazole planes of the different strands within each Eu(III) coordination sphere in contrast to those found for $[Eu(mbzimpy)_3]^{3+}$.[28]

The pseudo-D_3 cations $[Eu_2(L)_3]^{6+}$ are arranged with the Eu–Eu axis roughly along the *b* direction, but we do not observe a well-defined intermolecular columnar packing as described for $[Eu(mbzimpy)_3]^{3+}$.[28] The perchlorate anions and the solvent molecules are distributed around each $[Eu_2(L)_3]^{6+}$, filling the interstitial space between the triple-helical cations.

Table II. Reflectance Spectra (295 K, cm^{-1}, 5% in MgO, vs MgO], Emission Spectra (77 K, cm^{-1}, microcrystalline powders, λ_{ex} = 420 nm),[a] and Lifetimes (τ, ms) of $[Ln_2(L)_3](ClO_4)_6 \cdot n$solv Complexes (5–9)

Ln	$\pi_2 \rightarrow \pi^*$	$\pi_1{}^a \rightarrow \pi^*$	$\pi_1{}^b \rightarrow \pi^*$	$^1\pi\pi^*$	$^3\pi\pi^*$	τ
L	37 880	28 090		24 400	18 520	4.4
La	39 060	29 410	26 040	*b*	20 920	
					19 608	
					18 940	
					18 180	108
					17 390	
					16 530	
Eu	38 460	29 410	25 640	*c*	*c*	*c*
Gd	37 310	29 410	25 770	*25 970*	19 880	
				23 810	19 420	
					18 180	0.8
					17 330	
					16 530	
Tb	37 880	30 300	25 640	*c*	*c*	*c*

[a] The more intense component is italicized. [b] Too weak to be observed. [c] Not observed due to energy transfer onto the Ln ion.

Photophysical Properties of Crystalline $[Ln_2L_3](ClO_4)_6 \cdot n$solv (5–11). The ligand presents a broad and intense $\pi_1 \rightarrow \pi^*$ transition at 28 090 cm^{-1}, with a shoulder at 30 120 cm^{-1}. Upon complexation, the $\pi_1 \rightarrow \pi^*$ transition is split into two components[22,28] (Table II; Figure F1, supplementary material) separated by 3600 cm^{-1} (La, Eu, and Gd) and 4700 cm^{-1} (Tb) at 30 300 cm^{-1} (Tb) or 29 400 cm^{-1} ($\pi_1{}^a \rightarrow \pi^*$) and 25 600–26 000 cm^{-1} ($\pi_1{}^b \rightarrow \pi^*$). Another transition, $\pi_2 \rightarrow \pi^*$, is observed at 37 880 cm^{-1}, which is slightly displaced in the $[Ln_2L_3] \cdot n$solv complexes.

Excitation of the La and Gd complexes through the $\pi_1 \rightarrow \pi^*$ and $\pi_2 \rightarrow \pi^*$ transitions at 77 K results in emission spectra containing two broad bands (Figure 3, Table II). One, very weak, occurs between 29 000 and 21 000 cm^{-1}, and its lifetime is short; we assign it as arising from the $^1\pi\pi^*$ state. The second band extends from 21 000 to 15 000 cm^{-1}. It is structured, with a maximum at 18 200 cm^{-1} and lifetimes of 4.4 (L), 108 (La), and 0.8 (Gd) ms. It therefore originates from the $^3\pi\pi^*$ state. For the Eu, Tb, and mixed Eu–Tb complexes, the emission from the $^3\pi\pi^*$ state is completely quenched and the characteristic emission bands of Eu and Tb appear in the spectra, pointing to an efficient ligand-to-metal energy-transfer process (Figure 3).

We have examined the excitation and emission spectra of the Eu compound in great detail, in order to determine the influence of the hydration water. Three samples were measured. Two of them contained two (**6**, Eu-H2) and nine (**7**, Eu-H9) hydration water molecules, and the third was comprised of single crystals grown in CH_3CN/Et_2O, corresponding to the crystals used for X-ray analysis (**11**, Eu-C9). These samples have been investigated at 295 and 77 K (and at 4 K for Eu-H9) under excitation through the ligand ($\pi_1 \rightarrow \pi^*$) transition or through the Eu ($^5D_0 \leftarrow {}^7F_0$) transition. The excitation spectra at 77 K in the region of the $^5D_0 \leftarrow {}^7F_0$ transition (Figure F2, supplementary material) reveal significant differences. The band for Eu-H9 is broad; it appears at 17 220 cm^{-1} with a full width at half-height (fwhh) of 15 cm^{-1} and is asymmetric on the short wavelength side. The band for Eu-H2 is slightly more symmetrical but presents essentially the

(29) Shannon, R. D. *Acta Crystallogr.* **1976**, *A32*, 751.
(30) Constable, E. C. *Tetrahedron* **1992**, *48*, 10013–10059.
(31) Williams, A. F.; Piguet, C.; Bernardinelli, G. *Angew. Chem., Int. Ed. Engl.* **1991**, *30*, 1490.

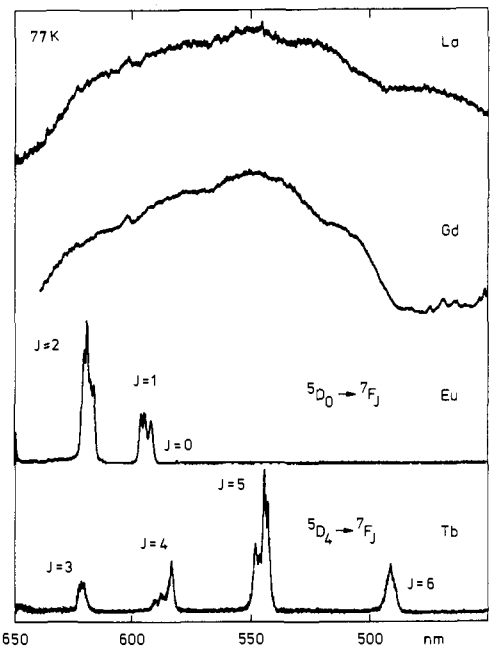

Figure 3. Emission spectra of the ligand for powdered samples of $[Ln_2L_3](ClO_4)_6$ (Ln = La, **5**; Eu, **7**; Gd, **8**; and Tb, **9**) complexes upon excitation at 420 nm ($\pi_1 \rightarrow \pi^*$ transition) at 77 K.

same features, while the band for Eu-C9 is symmetrical, appears at 17 226 cm^{-1}, and is sharper (fwhh = 10 cm^{-1}). These findings are confirmed by the observation of the $^5D_0 \rightarrow {}^7F_0$ transitions in the emission spectra, which present the following characteristics: 17 223 cm^{-1} (fwhh = 30 cm^{-1}) for Eu-H9, 17 220 cm^{-1} (15 cm^{-1}) for Eu-H2, and 17 227 cm^{-1} (10 cm^{-1}) for Eu-C9. The band profile of the 0–0 transition is indicative of how well defined is the Eu chemical environment:[3] fwhhs between 1 and 2 cm^{-1} are observed at 77 K for well-defined Eu sites,[32] while the bandwidth increases to 15–30 cm^{-1} when the compound contains a statistical distribution of molecules with somewhat different conformations.[33] Given the relative complexity of the ligand used here, one can deduce that the chemical environment of the Eu ion is reasonably rigid in the CH_3CN-containing crystals. Upon hydration, some interaction takes place, which apparently creates more distortion in the vicinity of the metal ion. One goal of the detailed spectroscopic study is to assess the nature of this interaction.

The band positions and intensities of the luminescence spectra of Eu-H2 and Eu-H9 are identical when excitation is through the ligand band (Table S2, supplementary material). Selective laser excitations through the profile of the 0–0 transitions do not reveal important differences between the emission spectra, except for the shifts expected in compounds in which the various molecules are probably distributed among several slightly different conformations.[33] The crystal field splittings reported in Table III and calculated from spectra measured after direct laser excitation to the $^5D_0$ level clearly show significant differences between the spectra of the hydrated samples Eu-H2 and Eu-H9 and the spectrum obtained with the single crystals Eu-C9 (Figure 4). The latter may be interpreted in terms of a pseudo-D_3 symmetry around the Eu(III) ion. The $^5D_0 \rightarrow {}^7F_0$ transition, which is symmetry forbidden in D_3, is extremely weak (Table S2, supplementary material). There are two main transitions to the $^7F_1$ level, $A_1 \rightarrow A_2$ and $A_1 \rightarrow E$, which are both allowed in D_3,

(32) Bünzli, J.-C. G.; Klein, B.; Chapuis, G.; Schenk, K. *Inorg. Chem.* **1982**, *21*, 808. Bünzli, J.-C. G.; Klein, B.; Wessner, D.; Alcock, N. W. *Inorg. Chim. Acta* **1982**, *59*, 269. Bünzli, J.-C. G.; Klein, B.; Plancherel, D.; Chapuis, G. *Helv. Chim. Acta* **1986**, *69*, 288.

(33) Bünzli, J.-C. G.; Pradervand, G. O. *J. Chem. Phys.* **1986**, *85*, 2489. Bünzli, J.-C. G.; Plancherel, D.; Pradervand, G. O. *J. Phys. Chem.* **1989**, *93*, 980. Plancherel, D.; Jin, L.; Massara, R.; Bünzli, J.-C. G. *Helv. Chim. Acta* **1987**, *70*, 1298. Nicolò, F.; Plancherel, D.; Chapuis, G.; Bünzli, J.-C. G. *Inorg. Chem.* **1988**, *27*, 3518.

Table III. Identified Eu(^7F_J) Energy Levels (cm^{-1}, J = 1–4) in $[Eu_2L_3](ClO_4)_6 \cdot n$solv complexes (6, 7, and 11), As Calculated from Luminescence Spectra at 77 K (λ_{ex} = 580.50 (Eu-C9), 580.71 (Eu-H2), and 580.62 (Eu-H9) nm)[a]

level	Eu-C9	Eu-H2	Eu-H9	level	Eu-C9	Eu-H2	Eu-H9
$^7F_0$	0	0	0		1871	1835	
$^7F_1$	295	303	307	$^7F_4$	2707	2697	2696
	413	376	395		2720	2723	2724
	431	400	436		2757		
$^7F_2$	1000	980	986		2766	2773	2776
	1029	1029	1019		2780		
			1039			2844	
	1086	1070	1070			2880	2877
	1096	1104	1102		2988	2986	2986
$^7F_3$	1819	1822	1829				

[a] Key: Eu-C9 = **11**, Eu-H2 = **6**, and Eu-H9 = **7**.

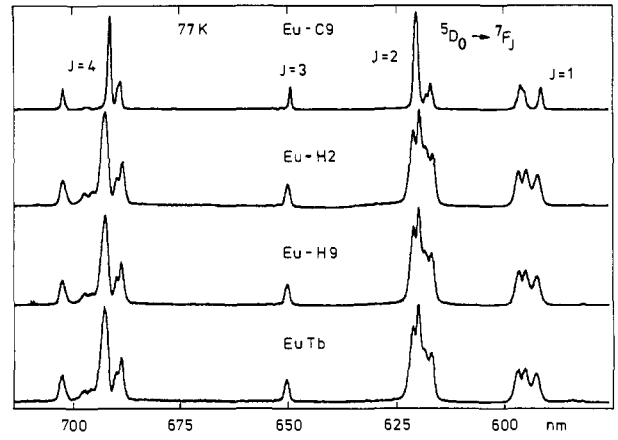

Figure 4. Part of the emission spectra at 77 K of microcrystalline samples of $[Eu_2L_3](ClO_4)_6 \cdot nH_2O$ (n = 9 and 2) and of single crystals of $[Eu_2L_3](ClO_4)_6 \cdot 9CH_3CN$ in CH_3CN/Et_2O (λ_{ex} = *ca.* 580.5 nm).

the latter being further broken up into two closely spaced components, separated by 18 cm^{-1}, as was observed for $[Eu(mbzimpy)_3](ClO_4)_3$[28] or for the $[Eu(terpy)_3]^{3+}$ complex.[34] The transition to the $^7F_2$ level is comprised of two main bands which are further split into two and three components. The additional splitting of the E components is again small, 30 and 10 cm^{-1}. One component of the short-wavelength triplet arises from a vibronic band (1013 cm^{-1}, Raman 1009 cm^{-1}). We therefore assign the two main bands of the $^5D_0 \rightarrow {}^7F_2$ transition to the two allowed electric dipole transitions $A_1 \rightarrow E$ in D_3 symmetry. This analysis is also consistent with the observed $^5D_0 \rightarrow {}^7F_4$ transition; two of the three main bands are split into two components (9 and 13 cm^{-1}) and are assigned to two of the three allowed $A_1 \rightarrow E$ transitions. The sharp band at 702.3 nm is tentatively assigned to the $A_1 \rightarrow A_2$ transition, while the broad, weak component around 692 nm could correspond to the third $A_1 \rightarrow E$ transition. Overall, the emission spectrum points to both Eu(III) ions having the same chemical and structural environment with a symmetry close to D_3.

For the hydrated complex Eu-H9, the crystal field splitting is substantially modified. The two $^7F_1$ sublevels arising from the E level in D_3 symmetry undergo a larger separation (41 *vs* 18 cm^{-1} for Eu-C9), and the gap between the lowest two levels is reduced to 88 cm^{-1}, from 118 cm^{-1} in Eu-C9, while the total splitting remains approximately the same, 129 *vs* 136 cm^{-1}. This is characteristic of a larger distortion from the pseudo-D_3 symmetry, with loss of the pseudo-C_3 axis. A similar trend is observed for $^7F_2$, with separations between the components of the E levels equal to 33 and 32 cm^{-1}. Examination of the crystal structure shows that the Eu(III) ions are not well shielded at the ends of the pseudo-C_3 axis. One water molecule could easily

(34) Durham, D. A.; Frost, G. H.; Hart, F. A. *J. Inorg. Nucl. Chem.* **1969**, *31*, 833.

Table IV. Lifetimes (ms) of the Eu($^5D_0$) and Tb($^5D_4$) Levels in $[Ln_2(L)_3](ClO4)_6$·*n*solv Complexes as a Function of Temperature and Excitation Wavelength (Standard deviations are indicated in parentheses)[a]

T/K	Eu-C9	Eu-H2	Eu-H9	Tb-C9	Tb-H3	Tb-Eu
			Selective Excitation			
4	*b*	*b*	1.78(8)	*b*	*b*	*b*
77	2.03(4)	2.04(5)	1.93(7)	1.35(4)	0.66(3)	0.66(2)[c] 0.16(2)[c]
140	2.11(10)	1.93(7)	1.82(8)	*b*	0.48(5)	*b*
205	1.84(7)	1.37(9)	1.15(4)	*b*	0.39(3)	*b*
250	0.63(7)	0.72(5)	0.30(1)	*b*	0.32(2)	*b*
295	*b*	0.24(1)	0.29(1)	*b*	*b*	*b*
			Excitation through the Ligand Band			
77	2.12(11)	2.36(6)	2.28(6)	1.24(6)	0.55(2)	0.71(4)[c] 0.20(1)[c]
295	1.62(4)	0.45(2)	0.45(3)	*b*	0.25(5)	*b*

[a] Key: Eu-C9 = **11**, Eu-H2 = **6**, Eu-H9 = **7**, Tb-C9 = **12**, and Tb-H3 = **9**. [b] Not measured. [c] Biexponential decay.

slide between the terminal benzimidazole groups and coordinate to the Eu(III) ions, which would then become 10-coordinate and lead to the observed features in the luminescence spectra. To investigate this interpretation, we have determined the lifetimes of the Eu($^5D_0$) and Tb($^5D_4$) states in the various samples (Table IV). At 77 K, the Eu-C9 crystals have a long lifetime, comparable to the one measured for the 1:3 complex with mbzimpy (1.85 ms)[28] and implying that the Eu environment is fairly rigid. Water is known to quench efficiently the Eu(III) luminescence *via* the high-energy OH vibration.[3] If one molecule of water coordinates onto the Eu(III) ion, the lifetime of the $^5D_0$ state should decrease from 2 ms to about 0.7 ms. Surprisingly, this is not the case; at 77 K, the lifetime remains essentially the same for Eu-H2 (2.04 ms), Eu-H9 (1.93 ms), and Eu-C9 (2.01 ms). We conclude that the water molecules do not coordinate onto the lanthanide ions but are, rather, hydrogen bonded to the ligand. The effect of these hydrogen bonds is a distortion which removes the trigonal symmetry of the helical complex, leading to the observed emission spectra. The situation for Tb compounds is different, the $^5D_4$ lifetime being sensitive to hydration. It drops from 1.35 ms in anhydrous crystals $[Tb_2(L)_3](ClO_4)_6$·$9CH_3CN$ (Tb-C9, **12**) to 0.66 ms in microcrystals containing three water molecules (Tb-H3). This drop would be expected if these water molecules were interacting in the inner coordination sphere.

The Eu($^5D_0$) lifetime remains approximately constant between 4 and 150 K and then decreases sharply to reach very short values at room temperature (Table IV). A similar behavior is observed for Tb-H3. This indicates a luminescence quenching by a large number of vibrational quanta from the ligand modes and, in the case of Eu, possibly by a ligand-to-metal charge-transfer state. Unfortunately, the absorption due to excitation of the ligand extends into the visible region and precludes the direct observation of the charge-transfer state. A final feature displayed by the Eu($^5D_0$) lifetime is its dependence upon the excitation mode; it is longer when the excitation occurs through energy transfer from the ligand (Table IV). The difference is small at 77 K but significant at room temperature. We therefore assess that the L → Eu energy transfer occurs *via* the ligand long-lived triplet state which acts as the rate-limiting factor in the entire light-conversion process.

The investigation of both a pure Tb complex and a mixed Eu–Tb compound (50–50% in the synthetic mixture) was undertaken in order to get further insight into the light-conversion processes and to determine the mechanism of the Tb → Eu energy transfer. The emission spectra of the Tb complex are dominated by the $^5D_4 \rightarrow {}^7F_5$ transition (Figure 3). The relative intensities of the $^5D_4 \rightarrow {}^7F_J$ transitions are 1.0, 2.7, 0.9, 0.5, and 0.03 for J = 6, 5, 4, 3, and 2, respectively. The total intensity of the emission spectrum is relatively weak, pointing to some back-transfer to the ligand, followed by nonradiative deexcitation, as

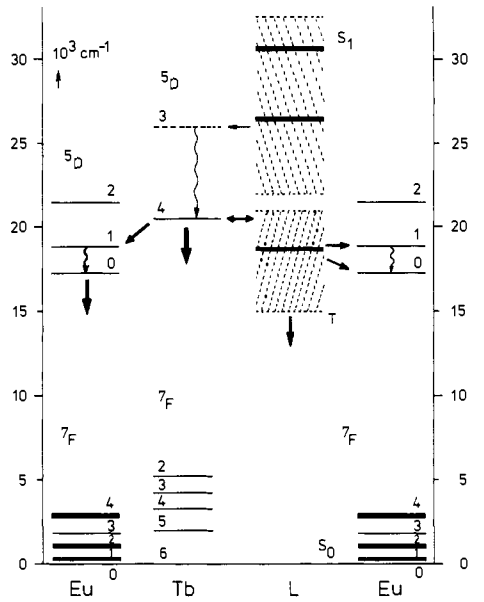

Figure 5. Energy-level scheme showing ground and excited states and intramolecular energy-transfer processes in homodinuclear $[Ln_2L_3](ClO_4)_6$·*n*solv (Ln = Eu and Tb) and heterodinuclear Eu–Tb complexes, as determined from luminescence data at 77 K.

has been observed for Tb cryptates[4,5] and for Tb(mbzimpy)$(NO_3)_3(CH_3OH)$.[28] This leads to a Tb($^5D_4$) lifetime considerably smaller than the one measured for Eu($^5D_0$), despite the larger energy gap $^5D_4$–$^7F_0$ as compared to $^5D_0$–$^7F_6$. Upon ligand excitation, the Tb–Eu mixed complex displays both the Eu and Tb emission spectra, the latter being, however, weaker (15% of the total Eu intensity). The Eu spectrum is identical with the ones observed for Eu-H2 and Eu-H9, indicating that the Ln sites have the same structural properties. On the other hand, the Tb($^5D_4$) luminescence decay is biexponential. One lifetime is identical with the lifetime of the homodinuclear Tb complex, while the other is shorter (Table IV) and arises from the heterodinuclear Eu–Tb complex since the mixed compound is in fact a mixture of homo-(Eu–Eu and Tb–Tb) and heteromolecules (Eu–Tb). The yield $\eta = 1 - \tau/\tau_0$ of the Tb → Eu transfer is 76%. If the mechanism of the energy-transfer process were dipole–dipolar, the following expression should hold:

$$\eta = 1 - \tau/\tau_0 = [1 + (R/R_0)^6]^{-1}$$

where τ is the Tb($^5D_4$) lifetime in the Eu–Tb complex, τ_0 is the lifetime in the pure Tb complex, R is the Eu–Tb distance, and R_0 is the critical distance for 50% transfer.[3] Using R = 8.876 Å, we find R_0 = 10.7 Å. Since for Eu–Tb pairs R_0 usually ranges between 8 and 10 Å,[3] we conclude that the transfer occurs *via* a dipole–dipolar mechanism. The same calculation made using the lifetimes determined upon ligand excitation yields η = 72% and R_0 = 10.4 Å.

The energy level scheme reported in Figure 5 summarizes the intramolecular energy-transfer processes taking place in $[Ln_2(L)_3](ClO_4)_6$·*n*solv (Ln = Eu and Tb).

Self-Assembly of $[Ln_2(L)_3]^{6+}$ in Solution (Ln = La, Eu, Gd, Tb, and Lu). Electrospray mass spectrometry (ES–MS) is particularly suitable for characterizing preformed ions in solution,[35] and we have recently shown that the ES–MS mass spectra of supramolecular complexes under low upfront CID reflect the distribution of the species formed in solution.[36] ES–MS mass spectra of complexes **5–10** in acetonitrile (5×10^{-5} M) display major peaks corresponding to the multiply charged cations $[Ln_2(L_3)]^{6+}$ (Ln

(35) Smith, R. D.; Loo, J. A.; Edmonds, C. G.; Barinaga, C. J.; Udseth, H. R. *Anal. Chem.* **1990**, *62*, 882.
(36) Hopfgartner, G.; Piguet, C.; Henion, J. D.; Williams, A. F. *Helv. Chim. Acta* **1993**, *76*, 1759.

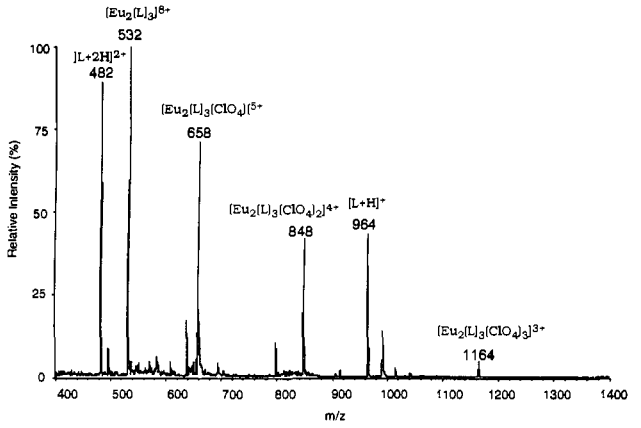

Figure 6. ES–MS spectrum of $[Eu_2(L)_3](ClO_4)_6$ (**6**, 5×10^{-5} M) in CH_3CN.

= La, Eu, Gd, Tb, and Lu) and the protonated ligands $[L + H]^+$ and $[L + 2H]^{2+}$ which strongly suggests a cooperative self-assembly process[37] for the formation of the dinuclear complexes. The observation of peaks corresponding to the protonated free ligand in the ES–MS mass spectrum of $[Ln_2(L)_3]^{6+}$ is in complete agreement with the excellent ES–MS response of the ligand L[36] and with a partial decomplexation of the complexes in these conditions, which is more pronounced for the heavier lanthanide ions since the intensities of the peaks corresponding to the cations $[Ln_2(L)_3]^{6+}$ drastically decrease when going from Ln = La to Lu. We were not able to detect the expected free metal under low declustering conditions, since various clusters with the solvent are normally obtained.[38] We also observed some smaller peaks corresponding to the species $[Ln_2(L)_3(ClO_4)_i]^{(6-i)+}$ (i = 1–3) where perchlorate anions are associated with the multiply charged cations (Figure 6). Associations between cations and ClO_4^- in solution[39] or in nitrobenzyl alcohol matrices[40] are well-documented, and we have attributed this effect to the high charge (6+) of the dinuclear cations.[36] Finally, we have used ES–MS to characterize the complexes obtained by mixing stoichiometric quantities of ligand (3 equiv) with $Ln^1(ClO_4)_3$ (1 equiv) and $Ln^2(ClO_4)_3$ (1 equiv) ($Ln^1 \neq Ln^2$; Ln = La, Eu, Gd, Tb, and Lu). In all cases, we only observed three different complexes in solution corresponding to the three expected dinuclear cations $[(Ln^1)_2(L)_3]^{6+}$, $[(Ln^1)(Ln^2)(L)_3]^{6+}$, and $[(Ln^2)_2(L)_3]^{6+}$ which strongly support strict self-assembly processes.[41] Given the partial decomplexation observed in the conditions of ES–MS measurements (approximately 15% for **5**–**7** and 30% for **10**, vide infra), it is not possible to compare the relative concentrations of hetero- and homodinuclear complexes with those obtained by ^1H NMR.

Spectrophotometric titrations of L with $Ln(ClO_4)_3 \cdot nH_2O$ (Ln = La, Eu, and Lu; n = 6 and 8) in acetonitrile (Ln:ligand ratio in the range of 0.15–1.67) show a sharp end point near a Ln:ligand ratio of 0.65. Isosbestic points are always observed during the titrations which implies the existence of only two absorbing species in solution for each titration. This result is confirmed by factor analysis,[20] and the spectrophotometric data can be satisfactorily fitted with a single equilibrium involving the dinuclear cations $[Ln_2(L)_3]^{6+}$:

$$3L + 2Ln^{3+} \leftrightarrow [Ln_2(L)_3]^{6+}$$

With a total concentration of 9.73×10^{-5} M for L and 6.49×10^{-5} M for Ln(III) (Ln:ligand ratio = 0.67), the Bjerrum complex formation functions[42] $\bar{n}$ for Ln = La and Eu reach a value of 1.3–1.4 which do not allow a very accurate determination of the stability constants which can be estimated to $20 \leq \log(\beta_{23}) \leq 22$; for Ln = Lu, $\bar{n} \leq 1.0$ in the same conditions leading to a more precise determination of $\log(\beta_{23}) = 17.5(4)$. This decrease in stability when going from Eu to Lu confirms the ES–MS measurements and parallels the behavior previously observed for the mononuclear complexes $[Ln(mbzimpy)_3]^{3+}$.[28]

Having established that $[Ln_2(L)_3]^{6+}$ are the only complexes formed in acetonitrile, we have investigated their structures in solution by ^1H NMR and luminescence. The ^1H-NMR spectra of the diamagnetic cations $[La_2(L)_3]^{6+}$ (**5**) and $[Lu_2(L)_3]^{6+}$ (**10**) both display 12 different signals for the aromatic protons in the range of 5.0–8.0 ppm. The methylene protons H_{11} and H_{12} remain enantiotopic upon complexation, but H_{13} and H_{14} clearly show AB spin systems as a result of intramolecular diastereotopic effects.[13] These features correspond to three equivalent ligands L coordinated to two lanthanide ions in triple-helical pseudo-D_3 cations[11] as similarly found for the mononuclear complex $[La(mbzimpy)_3]^{3+}$.[28] Two-dimensional homonuclear correlation spectra and comparison with $[La(mbzimpy)_3]^{3+}$ [28] allow the attribution of the ^1H-NMR signals given in Table V. Compared to the free ligands, the pyridine protons H_5–H_7 in **5** and **10** undergo significant upfield shifts (0.1–0.3 ppm for H_6 and 0.5–1.25 ppm for H_5 and H_7), in contrast to the expected downfield shifts resulting from N-coordination of the pyridine ring to positively charged ions.[10,22,28,43] A careful examination of the structure of **11** shows that H_5–H_7 are located in the shielding region of two aromatic benzimidazole rings belonging to the other strands of the triple-helix (Figure 2). An analogous effect was already reported for $[La(mbzimpy)_3]^{3+}$ [28] which suggests a similar wrapping of the strands around the metal ions in mononuclear and dinuclear triple-helical complexes.

The ^1H-NMR spectrum of the complex $[Eu_2(L)_3]^{6+}$ (**7**) also displays typical features of the triple-helical pseudo-D_3 symmetry of the cation (H_{11} and H_{12} enantiotopic; H_{13} and H_{14} diastereotopic) but spreads over 16 ppm as a result of the paramagnetic Eu(III) ions[44] (Figure 7). As previously observed for $[Eu(mbzimpy)_3]^{3+}$,[28] the protons close to the Eu(III) (H_1 and H_{10}) undergo significant downfield shifts together with a broadening of the signals due to dipolar interactions between the electronic and nuclear magnetic moments.[44] Finally, the ^1H-NMR spectrum of $[Tb_2(L)_3]^{6+}$ (**9**), although more broadened by paramagnetic effects, also confirms the existence of a triple-helical pseudo-D_3 cation in solution.

The absorption spectrum of the free ligand in acetonitrile displays a strong $\pi_1 \rightarrow \pi^*$ transition centered at 30 030 cm^{-1} which is split into two components ($\pi_1^a \rightarrow \pi^*$ and $\pi_1^b \rightarrow \pi^*$) upon complexation to Ln(III) as previously described for mbzimpy complexes.[22,25,28] The absorption band tails off into the visible, up to 410 nm, which prevents identification of a possible charge-transfer-state band in the case of the Eu complex. A solution of the anhydrous Eu complex in acetonitrile (10^{-3} M) yields only a weak luminescence spectrum, the intensity of which decreases by a factor of 3 if oxygen is bubbled into the solution. This proves that the energy-transfer process mainly takes place through the triplet state of the ligand. The emission bands are broad and present fewer maxima than in the solid state. Their general features are consistent with a pseudo-D_3 symmetry. The hypersensitive transitions to $^7F_2$ and $^7F_4$ are more intense than for **11** at room temperature (Table S2), while the Eu($^5D_0$) lifetime is the same, 1.67 ± 0.06 ms. The dehydrated Tb solution of

(37) Pfeil, A.; Lehn, J.-M. *J. Chem. Soc., Chem. Comm.* **1992**, 838. Garrett, T. M.; Koert, U.; Lehn, J.-M. *J. Phys. Org. Chem.* **1992**, *5*, 529.
(38) Blades, A. T.; Jayaweera, P.; Ikonomou, M. G.; Kebarle, P. *J. Chem. Phys.* **1990**, *92*, 5900.
(39) Bünzli, J.-C. G.; Mabillard, C. *Inorg. Chem.* **1986**, *25*, 2750. Bünzli, J.-C. G.; Kasparek, V. *Inorg. Chim. Acta* **1991**, *182*, 101.
(40) Miller, J. M. *Adv. Inorg. Chem. Radiochem.* **1984**, *28*, 1.
(41) Lindsey, J. S. *New J. Chem.* **1991**, *15*, 153.
(42) Hartley, F. R.; Burgess, C.; Alcock, R. M. *Solution Equilibria*; Ellis Horwood Limited: Chichester, 1980.
(43) Lavallee, D. K.; Baughman, M. D.; Phillips, M. P. *J. Am. Chem. Soc.* **1977**, *99*, 718.
(44) Bertini, I.; Luchinat, C. *NMR of Paramagnetic Molecules in Biological Systems*; Benjamin/Cummings Publishing Company Inc.: 1986, Chapter 10.

Table V. ^{1}H-NMR Shifts (with respect to TMS) for the Ligand L in $CDCl_3$ and Complexes $[Ln_2(L)_3]^{6+}$ (Ln = La, **5**; Eu, **7**; Tb, **9**; and Lu, **10**) in CD_3CN

compd	H_1	H_2	H_3	H_4	H_4	H_6	H_7	H_8	H_9	H_{10}	$H_{11,12}$	$H_{13,14}$
L	7.81		7.20–7.28		8.37	7.96	8.24	7.18	7.14	7.63	4.21	5.86
$[La_2(L)_3]^{6+}$	7.58	7.20	6.65	7.20	7.20	7.83	7.76	7.39	7.20	5.83	3.20	4.49, 5.33
$[Lu_2(L)_3]^{6+}$	7.40	7.20	6.72	6.68	7.12	7.64	7.78	7.53	7.15	5.22	3.26	5.10, 5.64
$[Eu_2(L)_3]^{6+}$	13.7	7.68	7.38	5.68	2.95	5.34	3.61	6.11	7.52	14.8	3.98	2.96, 3.10
$[Tb_2(L)_3]^{6+}$	−59	−2.0	9.4	13.2	22.2	15.9	13.9	7.3	6.8	−83	1.5	5.5, 5.8

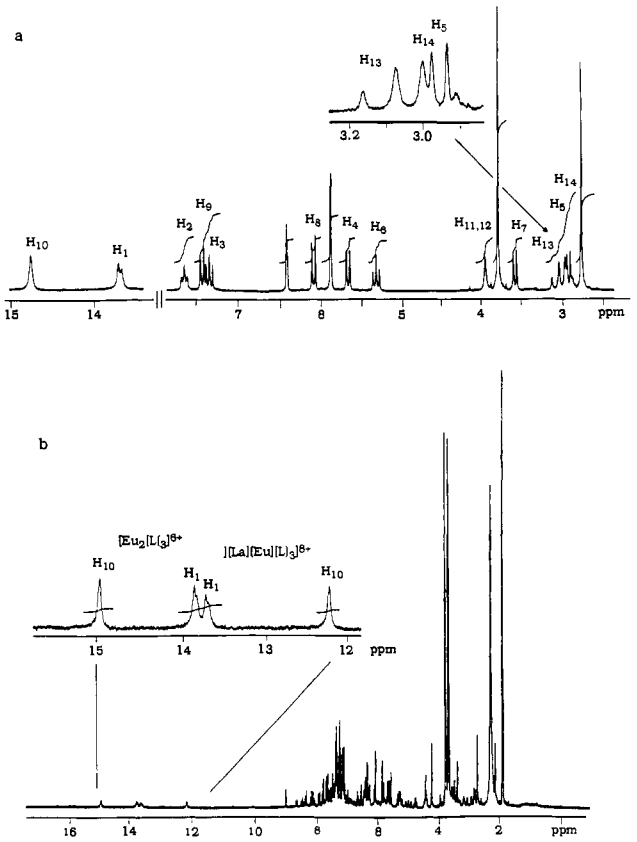

Figure 7. ^{1}H-NMR spectra of (a) $[Eu_2(L)_3]^{6+}$ in CD_3CN and (b) a mixture of L (3 equiv) with $La(ClO_4)_3$ (1 equiv) and $Eu(ClO_4)_3$ (1 equiv) in $CD_3CN/CDCl_3$ (9:1).

complex **9** shows only the $^5D_4 \rightarrow {}^7F_5$ transition in the emission spectra, and the Tb($^5D_4$) lifetime could not be determined.

Finally, we have used ^{1}H-NMR spectra to investigate more quantitatively the formation of self-assembled complexes $[(Ln^1)(Ln^2)(L)_3]^{6+}$ from mixtures of L, $Ln^1(ClO_4)_3$, and $Ln^2(ClO_4)_3$ in acetonitrile, since these heterodinuclear complexes are essential for the development of light-conversion molecular devices. A solution of L in $CD_3CN/CDCl_3$ (9:1, 2.2×10^{-2} M) was titrated with a concentrated solution containing equimolar quantities of $Ln^1(ClO_4)_3$ and $Ln^2(ClO_4)_3$ ($Ln^1 \neq Ln^2$; Ln = La, Eu, Tb, and Lu) in the same solvent. With an excess of ligand (Ln:ligand ratio < 0.6), we obtained very complicated ^{1}H-NMR spectra. A detailed analysis of the spectrum for Ln^1 = La and Ln^2 = Eu clearly shows the presence of the three previously characterized species L, $[La_2(L)_3]^{6+}$, and $[Eu_2(L)_3]^{6+}$ together with a fourth species displaying more than 29 different ^{1}H-NMR signals and corresponding to the heterodinuclear complex $[(La)(Eu)(L)_3]^{6+}$ previously characterized by ES–MS (significant overlaps between the signals in the spectrum prevent the attribution of the 34 expected protons, Figure 7). Very similar results are obtained for all the pairs of lanthanide studied (Table VI), but, in the case of Tb(III), broadening of the signals often prevents a very precise analysis of the ^{1}H-NMR spectra.

For a total metal-to-ligand ratio of 0.67, calculations with the stability constants given above show that less than 1% of the ligand is decomplexed, and we therefore do not detect any significant quantities of free ligand by ^{1}H NMR in contrast to the ES–MS results obtained under more dilute conditions. The ^{1}H-NMR spectra correspond to the mixture of the three expected self-assembled complexes. A detailed analysis based on the integrals of the ^{1}H-NMR signals allows one to estimate the distribution of species reported in Table VI. When Eu(III) is used, the situation is particularly favorable since the ^{1}H-NMR signals of the protons H_1 and H_{10} lie at low field and may be directly used to estimate the distribution of the species (Figure 7). Within experimental error, we always obtained the expected equimolar quantities of the homodinuclear complexes but only the La/Eu pair leads to the statistical formation (50%)[45] of the heterodinuclear complex. For the other pairs of lanthanide studied, we observed a significant systematic deviation from the statistical value toward lower quantities of $[(Ln^1)(Ln^2)(L)_3]^{6+}$ (Table VI). Since ^{1}H-NMR spectra do not change over a period of many weeks, this must reflect a thermodynamic rather than kinetic stability.

Table VI. Distribution of the Complexes Calculated from ^{1}H-NMR Spectra of Stoichiometric Mixtures of L (3 equiv) with $Ln^1(ClO_4)_3$ (1 equiv) and $Ln^2(ClO_4)_3$ (1 equiv) ($Ln^1 \neq Ln^2$; Ln = La, Eu, Tb, and Lu) in $CD_3CN/CDCl_3$ (9:1)[a]

Ln^1	Ln^2	% $[(Ln^1)_2(L)_3]^{6+}$	% $[(Ln^2)_2(L)_3]^{6+}$	% $[(Ln^1)(Ln^2)(L)_3]^{6+}$
La	Eu	25	25	50
La	Tb	36	36	28
La	Lu	35	35	30
Eu	Tb	33	33	34
Eu	Lu	35	35	30
Tb	Lu	35	35	30

[a] The error is typically ±3%.

With an excess of metal ions (Ln:ligand ratio > 0.7), we still only observed the three expected complexes in the ^{1}H-NMR spectra but the signals are slightly broadened probably as a result of exchange processes between free and coordinated lanthanide ions. The most stable homodinuclear complex is obtained preferentially, and the quantitative analysis of the distribution of the species allows a direct comparison of the relative stabilities of the complexes $[Ln_2(L)_3]^{6+}$. We obtained the following in decreasing order of stability: $[La_2(L)_3]^{6+} \cong [Eu_2(L)_3]^{6+} > [Tb_2(L)_3]^{6+} \gg [Lu_2(L)_3]^{6+}$, in good qualitative agreement with the ES–MS results and the spectrophotometric titrations.

Discussion

ES–MS spectra and spectrophotometric titrations in acetonitrile clearly show that the dinuclear species $[Ln_2(L)_3]^{6+}$ is the only complex formed when L is mixed with $Ln(ClO_4)_3$ which strongly suggests a cooperative strict self-assembly[41] as recently demonstrated for double-helicates with Cu(I) and Ag(I).[37] Similar processes are observed for all the lanthanides studied (Ln = La, Eu, Gd, Tb, and Lu), but the stability of the complexes $[Ln_2(L)_3]^{6+}$ significantly decreases for the heavier lanthanides. Competition between two different Ln(III)s with the ligand L shows that $[Ln_2(L)_3]^{6+}$ (Ln = La and Eu) have comparable stability, while $[Tb_2(L)_3]^{6+}$ and particularly $[Lu_2(L)_3]^{6+}$ are significantly less stable. The lifetime measurements on solid-state complexes confirm this trend; water does not interact in the

(45) Sharma, V. S.; Schubert, J. J. *J. Chem. Educ.* **1969**, *46*, 506. Sigel, H. *Angew. Chem., Int. Ed. Engl.* **1975**, *14*, 394.

inner coordination sphere of Eu, while it does for Tb. A rather similar discrimination effect, based on the size of the lanthanide ion and attributed to sterical constraints in the helical structure (intramolecular stacking interactions), was previously reported for the triple-helical mononuclear complexes $[Ln(mbzimpy)_3]^{3+}$.[28]

The ^{1}H-NMR spectra of $[Ln_2(L)_3]^{6+}$ imply a cation with pseudo-D_3 symmetry in solution, and the X-ray crystal structure of **11** confirms the triple-helical structure adopted by the cation $[Eu_2(L)_3]^{6+}$ where each Eu(III) is coordinated by nine nitrogen donor atoms in a very similar way as found for the mononuclear $[Eu(mbzimpy)_3]^{3+}$.[28] Thus, the structure of $[Eu_2(L)_3]^{6+}$ may be roughly derived from the packing of two $[Eu(mbzimpy)_3]^{3+}$ units along the helical axis. Compared to $[Eu(mbzimpy)_3]^{3+}$,[28] the ligand strands undergo a significant slipping in the dinuclear structure (Figure 2) which removes strong stacking interactions between the different strands within each Eu(III) coordination unit and gives some flexibility to the terminal aromatic benzimidazole rings. These observations strongly suggest that the ligand coordination cavities are less rigid for $[Ln_2(L)_3]^{6+}$ than for $[Ln(mbzimpy)_3]^{3+}$ which leads to less drastic discrimination effects based on the size of the coordinated lanthanide ions.[28] This is exemplified by the strict self-assembly and easy isolation of the triple-helical complex $[Lu_2(L)_3](ClO_4)_6$ (**10**), while only nonhelical $[Lu(mbzimpy)_2](H_2O)(CH_3OH)](ClO_4)_3$ was obtained.

The observation of less than statistical amounts of the heterodinuclear complexes when there is a significant difference in size between the two lanthanide ions and when at least one ion is smaller than Eu(III) is an indication that the organization of the ligands around the first metal ion leads to formation of a second coordination site more favorable for a second lanthanide ion of similar size.

The luminescent properties of the $[Ln_2L_3](ClO_4)_6 \cdot n$solv complexes (Ln = Eu for **6**, **7**, and **11** and Tb for **8**) show that the lighter Ln(III) ions are well protected by the helix-shaped ligand, as demonstrated by the long Eu($^5D_0$) lifetimes at low temperature. For Tb, however, water molecules can slip between the end parts of the ligands and interact with the metal ion. The ligand to lanthanide energy transfer is efficient and goes through the $^3\pi\pi^*$ state. For the Tb complex, this significant antenna effect is offset by a metal-to-ligand back-transfer (Figure 5). In absence of water, the emission spectra of the Eu(III) ion reflect a pseudo-trigonal symmetry around the metal ions, consistent with the crystal structure determination. One notes that the crystal field splitting of the Eu-containing compounds proves to be very sensitive to outside interaction with water molecules, which reinforce their potential use as sensors.

Conclusions

The criteria developed for the self-assembly of supramolecular helical complexes controlled by a metal ion stereochemical preference[11,30,46] are not limited to d-transition metal ions but may be successfully applied to the 4f lanthanide ions. Firstly, the ligand L possesses two well-defined metal binding sites separated by a spacer which is (i) flexible enough to allow efficient binding of the tridentate units to the metal ions, (ii) rigid enough to limit the number of possible conformations, and (iii) designed to dispose the binding sites in such a way as to favor the formation of helical multinuclear complexes.[11] Secondly, the binding possibilities of the ligand match the stereochemical preference of the metal ion. For the large lanthanide ions, high coordination number (CN = 8–10) are an essential requirement to prevent coordination of other ligands (solvent or anion)[3,22] which could hinder the self-assembly process and quench the luminescence of the resulting supermolecule. The ligand L is ideally suited for this purpose since it only can act as a bis(terdentate) unit,[11] and the use of three such ligands leads to 9-coordinated metal ions which are very common for Ln(III).[3] The resulting strict self-assembled triple-helical $[Ln_2(L)_3]^{6+}$ are, to the best of our knowledge, the first dinuclear helical supramolecular complexes containing luminescent 4f metal ions in highly symmetrical environments and working as light-conversion molecular devices. With respect to their possible use as luminescent probes, the main disadvantage of these complexes is the marked quenching they undergo at room temperature. Its origin lies in an insufficient rigidity of the ligand. Modification of L to rigidify the ligand backbone and protect the ends of the triple-helices from solvent-molecule and/or anion interaction should improve the luminescence quantum yield.

These complexes present an important theoretical interest. Their structure ensures that metal-to-metal energy transfers are restricted to intramolecular processes, which allows one to test the validity of the dipole–dipolar mechanism. The observed yield of the Tb → Eu energy-transfer process in the heterodinuclear complex points to the validity of the dipole–dipolar mechanism. The recognition of the fine structural effects responsible for the control of the formation of the heterodinuclear complexes in solution offers promising possibilities for the design of well-defined supramolecular light-conversion devices. Modifications of the ligand to provide different coordination sites for the metal ions and various metal–metal distances should allow further investigations of the dipole–dipolar mechanism of intramolecular energy transfers.

Acknowledgment. We gratefully acknowledge Ms. Véronique Foiret and Mr. Bernard Bocquet for their technical assistance. J.-C.B. thanks the Fondation Herbette (Lausanne) for the gift of spectroscopic equipment. This work is supported through grants from the Swiss National Science Foundation.

Supplementary Material Available: Table of atomic coordinates, bond distances, and bond angles for $[Eu_2(L)_3](ClO_4)_6(CH_3CN)_9$, table listing the luminescence intensities of the Eu complexes at various temperatures, reflectance spectra of L and complexes **5**–**10**, $^5D_0 \leftarrow {}^7F_0$ excitation spectra of complexes **6**, **7**, and **11**, and emission spectra at 77 K of microcrystalline samples of $[(Eu)(Tb)(L)_3](ClO_4)_6$ (16 pages). Ordering information is given on any current masthead page.

(46) Youinou, M.-T.; Ziessel, R.; Lehn, J.-M. *Inorg. Chem.* **1991**, *30*, 2144.